

## ESO Phase 3 Data Release Description

<b>Data Collection</b>	KiDS
<b>Release Number</b>	3
<b>Data Provider</b>	Konrad Kuijken
<b>Date</b>	18.07.2016

## Abstract

This data release constitutes the third public release by the Kilo-Degree Survey (KiDS). KiDS is an ESO public survey carried out with the VLT Survey Telescope and OmegaCAM camera, that will image 1500 square degrees in four filters (u, g, r, i), in single epochs per filter. KiDS is designed to be a weak lensing shear tomography survey, and has as its core science drivers mapping of the large-scale matter distribution in the universe and constraining the equation-of-state of Dark Energy. Secondary science cases are manifold and range from galaxy evolution to Milky Way structure, and from detection of white dwarfs to high-redshift quasars. This third data release can be considered an incremental release. The same types of data products are provided as in the second data release for an additional set of survey tiles (calibrated, stacked images and their weights, as well as masks and single-band source lists extracted from the stacks). Furthermore, a multi-band source catalogue is provided that encompasses the combined area of data releases 1, 2 and 3, for a total of 440 square degrees, observed in all filters. The data were taken under ESO programme IDs: 177.A-3016(A), 177.A-3016(B), 177.A-3016(C), 177.A-3016(D), 177.A-3016(E), 177.A-3016(G), 177.A-3016(J), 177.A-3016(K), 177.A-3017(A), and 177.A-3018(A).

## Overview of Observations

This data release (KiDS-ESO-DR3) consists of the coadded images, weight maps, masks and source lists of 292 survey tiles, adding to the 148 tiles released previously (50 in KiDS-ESO-DR1 and 98 in KiDS-ESO-DR2). Furthermore, KiDS-ESO-DR3 contains a multi-band source catalogue encompassing all publicly released tiles, a total of 440 survey tiles. Figure 1 shows the locations of these tiles within the KiDS fields. Partial observations for many of the other fields exist as well and will be included in future releases once their wavelength coverage is complete.

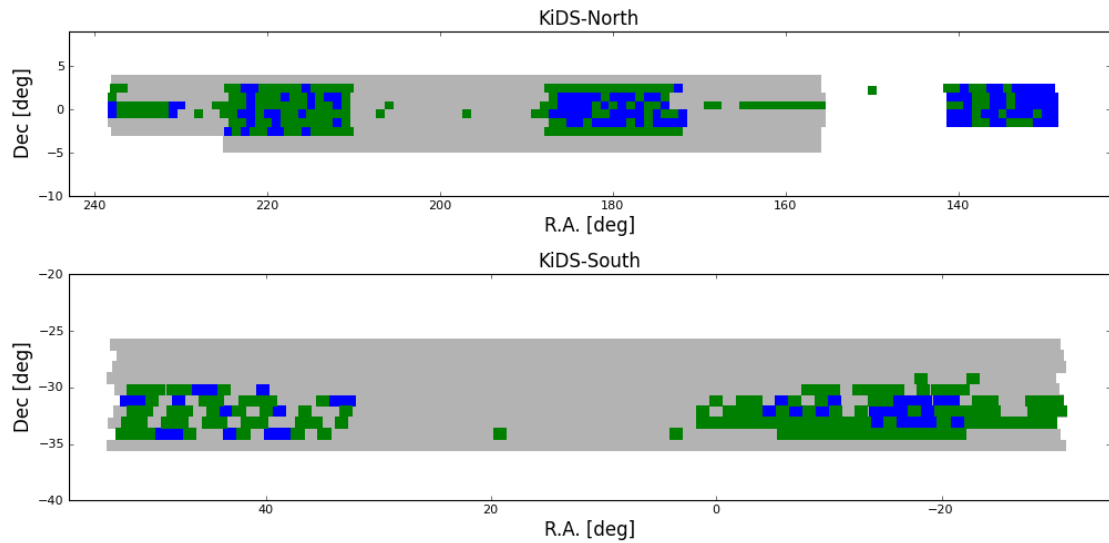


Figure 1: location of the 148 KiDS-ESO-DR1/DR2 tiles (blue) and the 292 KiDS-ESO-DR3 tiles (green); the KiDS survey area (top: KiDS-North; bottom: KiDS-South) is outlined in grey.

## Release Content

### Imaging products and single-band source lists

The complete list of 292 tiles for which imaging data products and single-band source lists are included in KiDS-ESO-DR3 is provided online: [http://kids.strw.leidenuniv.nl/DR3/data\\_table.php](http://kids.strw.leidenuniv.nl/DR3/data_table.php)

Each tile was observed in u, g, r, and i band. The final footprint of each tile is slightly larger than 1 square degree due to the dithering scheme: 61.9x65.4 arcminutes in u; 62.3x66.8 arcminutes in g, r and i. Taking this into account, the total sky coverage is approximately 320 square degrees, which is not contiguous, as illustrated in Figure 1.

The single-band source lists were extracted from the calibrated, stacked images for each tile and filter separately.

Since the OmegaCAM CCD mosaic consists of 32 individual CCDs, the sky covered by a single exposure is not contiguous but contains gaps. In order to fill in these gaps, KiDS tiles are built up from 5 dithered observations in g, r and i and 4 in u. The dithers form a staircase pattern with dither steps of 25'' in X (RA) and 85'' in Y (DEC), bridging the inter-CCD gaps (de Jong et al., 2015, A&A, 582, A62). The tile centres are based on a tiling strategy that tiles the full sky efficiently for VST/OmegaCAM. Neighbouring dithered stacks have an overlap in RA of 5% and in DEC of 10%.

In Figure 2 the obtained seeing (FWHM), PSF ellipticity, and limiting magnitude ( $5\sigma$  AB in 2'' aperture) distributions per filter are shown, to illustrate the obtained data quality. In case of the filters observed in dark time (u, g, r) the FWHM distributions reflect the different observing constraints, with r-band taking the best conditions. Since i-band is the only filter observed in bright time, it is observed under a large range of seeing conditions. Average PSF ellipticities are always small:  $<0.1$  (the average is over the absolute amount of ellipticity, regardless of the direction of ellipticity). The wide range of limiting magnitudes in i-band is caused by the large range seeing and in moon phase and thus sky brightness.

For a full overview of the data quality parameters for each observation we refer to the following online table: [http://kids.strw.leidenuniv.nl/DR3/data\\_table.php](http://kids.strw.leidenuniv.nl/DR3/data_table.php)

This part of the data release consists of 4672 files and a total data size of 3.6 TB.

### Multi-band source catalogue

Also included in KiDS-ESO-DR3 is a multi-band source catalogue. This source catalogue is based not only on the imaging data products described above, but also encompasses the tiles released in the previous data releases of KiDS (KiDS-ESO-DR1 and KiDS-ESO-DR2). Here we provide a general description of the catalogue data, while an overview of all tiles with coordinates, PSF size, limiting magnitude, etc. is provided online: [http://kids.strw.leidenuniv.nl/DR3/catalog\\_table.php](http://kids.strw.leidenuniv.nl/DR3/catalog_table.php)

The catalogue is based on a total of 440 survey tiles, providing a total area coverage of approximately 470 square degrees. Figure 2 shows the PSF sizes, average ellipticities and limiting magnitudes for all tiles included in the catalogue. As for the imaging products the overall image quality is best in r-band. For this reason the r-band data were used for the object detection for the catalogue. Subsequently, SExtractor was run in double-image mode to measure source parameters in the other filters. The star-galaxy classification included in the catalogue is also based on the r-band data. Photometric calibration of the catalogue was homogenized within the available contiguous patches (Fig. 1). Using stellar locus regression, the g- and i-band were calibrated to the r-band in each tile, and the r-band photometry was homogenized using the overlaps between the survey tiles. Since the stellar locus regression works less well for u-band, the u-band photometry was homogenized separately, again using tile overlaps, to yield the best multi-band calibration. To

assess the quality of this calibration scheme, zero-point offsets w.r.t. SDSS are calculated for all tiles in KiDS-North and also provided in the table linked above. Also provided in the catalogue are so-called Gaussian Aperture and Photometry (GAaP) magnitudes that are specifically designed to provide accurate colours of galaxies, and that approach PSF-fitting magnitudes for point sources. Photometric redshifts based on the GAaP magnitudes and the Bayesian BPZ method are included as well.

The catalogue contains a total of 48,736,591 sources, is made up of 441 files (440 data files and 1 metadata file), and has a total data volume of 37 GB.

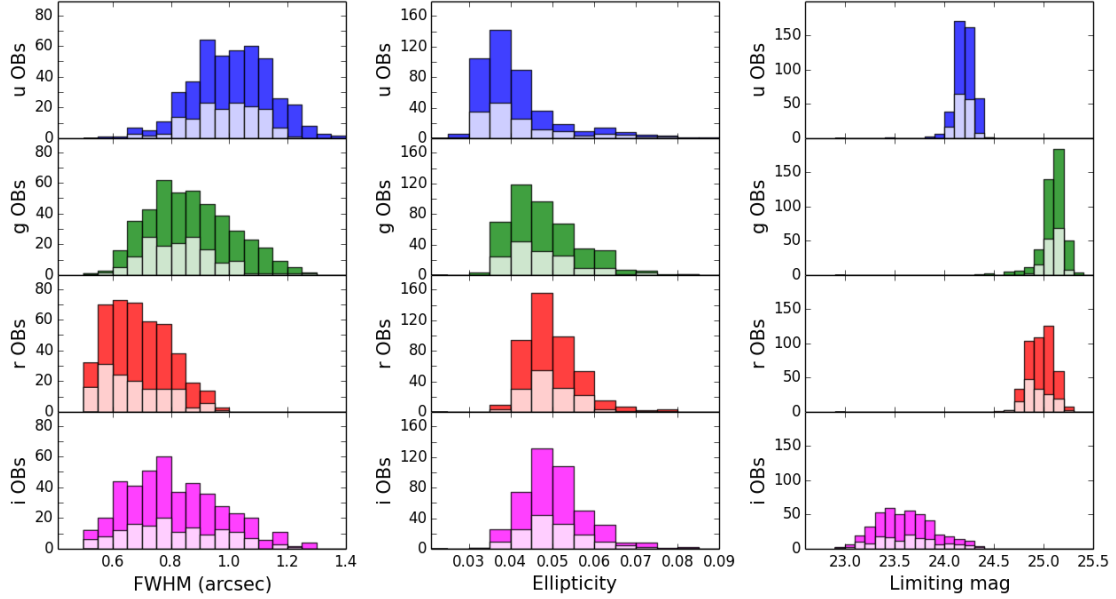


Figure 2: obtained raw data quality parameters for KiDS-ESO-DR1, -DR2 and -DR3. The light coloured portions of the histograms correspond to the 148 tiles in KiDS-ESO-DR1 and -DR2, and the dark coloured portions to the 292 tiles newly released in KiDS-ESO-DR3; the multi-band catalogue combines all 440 tiles and therefore corresponds to the total histograms. **Left:** average PSF size (FWHM) distributions; **centre:** average ellipticity distributions; **right:** limiting magnitude distributions ( $5\sigma$  AB in  $2''$  aperture). The distributions are per filter: from top to bottom u, g, r, and i, respectively.

## Release Notes

### Data Reduction and Calibration

The KiDS-ESO-DR3 pipeline is for the most part identical to the KiDS-ESO-DR2 pipeline (De Jong et al, 2015, A&A 582, A62) (DJ15) and based on the Astro-WISE optical pipeline described in McFarland et al. (2013, ExA 35, 79) (MF13). Below we summarize the processing steps and list KiDS-specific information (i.e., KiDS process configuration and departures from Astro-WISE optical pipeline). The main differences with the previous release occur in the multi-band source catalog, in which for the first time homogenized photometry, colour information and photometric redshifts are provided.

#### Image de-trending

De-trending of the raw data consists of the following steps.

- **Cross-talk correction.** Electronic cross-talk occurs between CCDs #93, #94, #95 and #96, resulting in faint imprints of bright sources on neighbouring CCDs. A correction was made for cross-talk between CCDs #95 and #96, where it is strongest (up to 0.7%).

- **De-biasing and overscan correction.** First, for each science and calibration exposure the overscan is subtracted per row (using method 6, see MF13). Second, a daily overscan-subtracted bias is subtracted. This is a daily average of 10 biases with  $3\sigma$ -rejection.
- **Flat-fielding.** Whereas in the two previous data releases a single masterflat (per CCD and filter) was used for all data, changes to the telescope baffles in three steps during 2014 necessitated the creation of new sets of masterflats. Table 1 lists the four different baffle configurations and the periods during which they were on the telescope.

Config.	Description	Start date	End date
1	Original set-up	May 2011	7 Jan 2014
2	Baffle extensions 1 (M2, chimney)	8 Jan 2014	6 Apr 2014
3	Baffle extensions 2 (M2, chimney, M1 plug)	7 Apr 2014	29 Apr 2015
4	Baffle extensions 3 (chimney ridges, plug)	30 Apr 2015	present

Table 1: VST baffle configurations

For each baffling configuration a single masterflat (per CCD and filter) was used, by virtue of the stability of the intrinsic pixel sensitivities, that can be considered constant to  $\sim 0.2\%$  or better for g, r and i (DJ15, Verdoes Kleijn et al., 2013, ExA, 35, 103). For g, r and i this master flat is a combination of a master dome (for high spatial frequencies) and master twilight (=sky) flat-field (for low spatial frequencies). Both contributing flats are an average of 5 raw flat-field exposures with  $3\sigma$ -rejection. In u band only the twilight flats are used.

- **Illumination correction.** Illumination correction (a.k.a. “photometric superflat”) is applied *in pixel space*, and only on the source fluxes (i.e., after background subtraction). A single illumination correction image is used to correct each masterflat (see also DJ15 and Verdoes Kleijn et al., 2013, ExA 35, 103). For baffling configuration 2, 3 and 4 illumination correction frames were derived from those for configuration 1, based on the difference between flatfields observed with each baffling configuration and with the original set-up.
- **De-fringing.** De-fringing is only needed for KiDS i-band. Analysis of nightly fringe frames showed that the pattern is constant in time. Therefore, a single fringe image was used for all KiDS-ESO-DR3 images observed after 2012-01-11. For each science exposure this fringe image is scaled (after background subtraction of the science exposure and fringe frame) and then subtracted to minimize residual fringes.
- **Pixel masking.** Cosmic-rays, hot and cold pixels, saturated pixels are automatically masked as described in MF13 during de-trending. These are included in the weight image. Additional automatic and manual masking is applied on the coadds (see below).
- **Satellite track removal.** Satellite tracks are detected automatically by applying the Hough transform (Hough, 1962) to a difference image of maximally overlapping exposures within a dither sequence after masking bright stars and bright ghosts. The pixels affected by satellite tracks are masked and included in the weight image.
- **Background subtraction.** To remove vignetting by bond wire baffling (Iwert et al. 2006, Proc. SPIE 6276, 62760A) in the focal plane, a row-by-row background subtraction method is used, before the background subtraction done by SWARP (see below).

### Photometric calibration

The steps taken to calibrate the photometry are as follows.

- KiDS-ESO-DR3 photometric calibration starts with individual zero-points per CCD based on SA field observations. The calibration deploys a fixed aperture (6.3 arcsec diameter) not corrected for flux losses, and uses SDSS DR8 PSF magnitudes of stars in the SA fields as reference. Magnitudes are expressed in AB in the instrumental photometric system (i.e., no colour corrections between OmegaCAM and SDSS photometric system applied).
- Next, the photometry in the g, r, and i filters is homogenized across CCDs and dithers for each filter in each tile independently. For u-band this homogenization is not applied because the relatively small source density often provides insufficient information to tie adjacent CCDs together. This global photometric solution is derived and applied in three steps:
  1. From the overlapping sources across dithered exposures, zero-point differences between the dithers (e.g. due to varying atmospheric extinction) are derived.
  2. Zero-point differences between CCDs are calculated using all CCD overlaps between the dithered exposures. Steps 1 and 2 both apply a minimization algorithm (see Maddox et al. 1990, MNRAS, 246, 433).
  3. The zero-point offsets are applied to all CCDs w.r.t. an average zero-point valid for the night, derived from the nightly SA field observations. If no SA field observations are available for the night, default values are used instead.

The above steps complete the photometric calibration of the image data and single-band source lists. A further homogenization of the photometry over the whole survey area is calculated using, and applied to, the multi-band source catalog, and is described below.

### Astrometry, regridding and coadding

A global (multi-CCD and multi-dither) astrometric calibration is calculated per filter per tile. SCAMP (Bertin 2006, ASP Conf. Series 351, 112) is used for this purpose, with a polynomial degree of 2 over the whole mosaic. The (unfiltered) 2MASS-PSC (Skrutskie et al. 2006, AJ, 131, 1163) is used as astrometric reference catalogue. A more detailed description of the astrometric pipeline is in MF13.

SWARP is used to resample all exposures in a tile to the same pixel grid, with a pixel size of 0.2 arcseconds. After background subtraction the exposures are coadded using a weighted mean stacking procedure.

### Masking of bright stars

A stand-alone program dubbed Pulecenella v1.0 (DJ15) was developed to create masks for KiDS coadds, and is now embedded in the pipeline. It is an automatized procedure for mask creation completely independent from external star catalogues. An example of a detail of a mask is shown in Figure 3. Pulecenella detects the following types of critical areas, all related to bright stars:

- saturated pixels,
- spikes caused by diffraction by the mirror supports,
- readout spikes,
- reflection halos produced by the optics components (a central core halo, and up to three wider reflection halos with spatially dependent offsets, depending on the brightness of the star).

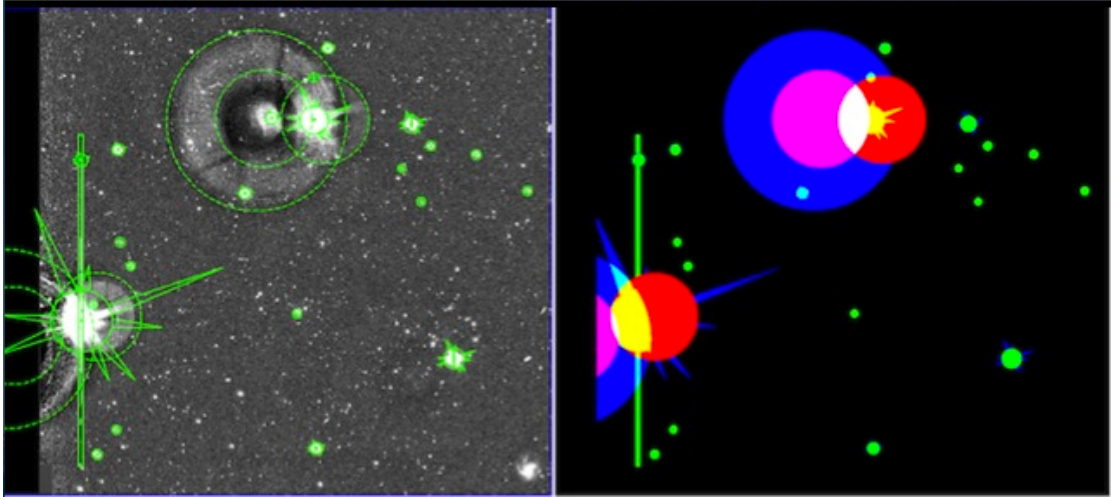


Figure 3: Detail of a Pulecenella v1.0 mask. **Left:** detail of a KiDS stacked image with bright stars; critical areas detected by Pulecenella are over-plotted with green outlines. **Right:** FLAG image corresponding to the image shown on the left, with different colours indicating the pixel values resulting from the combination of different flag values.

The masks are provided as FITS FLAG images, where each type of critical region is identified by a different flag value, as listed in Table 2. During source extraction for the single-band source list (see below) the FLAG image is used to flag sources whose isophotes overlap with the critical areas. The resulting flags are stored in the following two source parameters:

- IMAFLAGS\_ISO: FLAG image flags OR'd over the isophote profile
- NIMAFLAG\_ISO: number of flagged pixels entering IMAFLAGS\_ISO

Type of area	Flag value	Type of area	Flag value
Readout spike	1	Secondary halo	16
Saturation core	2	Tertiary halo	32
Diffraction spike	4	Bad pixel	64
Primary halo	8		

Table 2: Critical areas in the masks and their flag values.

#### Masking of image defects

Defects that are not related to bright stars, such as satellite tracks (if missed by automated masking during de-trending) or other artefacts, are not detected by Pulecenella. While for KiDS-ESO-DR1 and -DR2 these areas were masked by hand and included in the final masks, this has not been done for KiDS-ESO-DR3, due to the significantly larger data set. An alternative, automated procedure to detect and mask these types of areas is under active development, but still in an experimental state at the time of delivery of KiDS-ESO-DR3. Another advantage these masks will have over the manual masking provided in the previous releases, is increased homogeneity and objectivity, and the ability to release improved versions straightforwardly. These additional masks will be released on the KiDS-ESO-DR3 website (<http://kids.strw.leidenuniv.nl/DR3>) in due course.

#### Single-band source list extraction and star/galaxy separation

The single-band source lists delivered in this data release are intended as “general purpose” source lists. Source list extraction and star/galaxy (hereafter S/G) separation is done with an au-

tomated procedure optimized for KiDS data: KiDS-CAT. This procedure, the backbone of which is formed by S-Extractor (Bertin & Arnouts, 1996, A&AS, 317, 393) performs the following steps.

1. S-Extractor is run on the stacked image to measure the FWHM of all sources. High-confidence star candidates are then identified (for details see La Barbera et al. 2008, PASP, 120, L681).
2. The average PSF FWHM is calculated by applying the bi-weight location estimator to the FWHM distribution of the high-confidence star candidates.
3. A second pass of S-Extractor is done with SEEING\_FWHM set to the derived average PSF FWHM. During this second pass the image is background-subtracted, filtered and thresholded “on-the fly”. Detected sources are then de-blended, cleaned, photometered, and classified. A number of S-Extractor input parameters are set individually for each image (e.g., SEEING\_FWHM and GAIN), while others have been optimized to provide the best compromise between completeness and spurious detections (see Data Quality section below). The detection set-up used is summarized in Table 3; a full S-Extractor config file is available at this URL:

[http://kids.strw.leidenuniv.nl/DR3/example\\_config.sex](http://kids.strw.leidenuniv.nl/DR3/example_config.sex)

Apart from isophotal magnitudes and Kron-like elliptical aperture magnitudes, a large number of aperture fluxes are included in the source lists. This allows users to estimate aperture corrections and total source magnitudes. All parameters provided in the source lists are listed in the Data Format section below.

4. S/G separation is performed based the CLASS\_STAR (star classification) and SNR (signal-to-noise ratio) parameters provided by S-Extractor and consists of the following steps:
  - In the SNR range where the high-confidence star candidates are located (the red dots in Figure 4) the bi-weight estimator is used to define their CLASS\_STAR location,  $\theta$ , and its width,  $\sigma$ ; a lower envelope of  $\theta - 4\sigma$  is defined.
  - At SNR below that of the high-confidence star candidates, a running median CLASS\_STAR value is computed from sources with CLASS\_STAR > 0.8, which is shifted to match the  $\theta - 4\sigma$  locus. The resulting curve (blue curve in Figure 4) defines the separation of stars and galaxies.

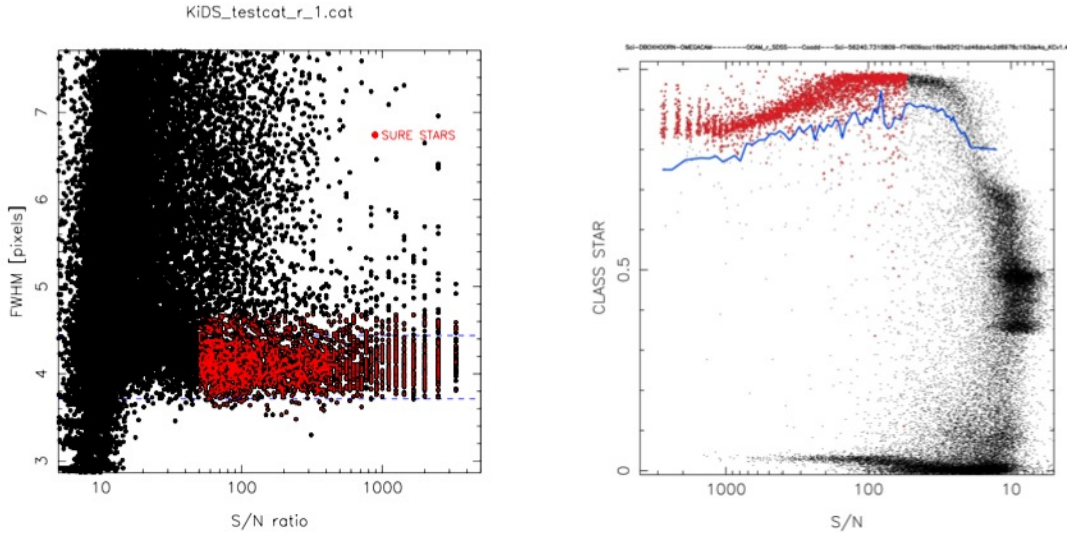


Figure 4: High-confidence star candidates and star/galaxy separation. **Left:** the high-confidence star candidates (red dots) are used to locate the stellar locus and calculate the average FWHM of the image. **Right:** example of star/galaxy separation; at SNR > 50, the high-confidence star candidates (red dots) are used to define the blue line; at lower SNR, all sources with CLASS\_STAR > 0.8 are used; sources above the blue line are classified as stars.

Parameter	Value	Description
DETECT_THRESH	1.5	<sigmas> or <threshold>,<ZP> in mag.arcsec-2
DETECT_MINAREA	3	minimum number of pixels above threshold
ANALYSIS_THRESH	1.5	<sigmas> or <threshold>,<ZP> in mag.arcsec-2
DEBLEND_NTHRESH	32	Number of de-blending sub-thresholds
DEBLEND_MINCONT	0.002	Minimum contrast parameter for de-blending
FILTER	Y	Apply filter for detection (Y or N)
FILTER_NAME	default.conv	Name of the file containing the filter
CLEAN	Y	Clean spurious detections? (Y or N)?
CLEAN_PARAM	1.0	Cleaning efficiency
BACK_SIZE	256	Background mesh: <size> or <width>,<height>
BACK_FILTERSIZE	3	Background filter: <size> or <width>,<height>
BACKPHOTO_TYPE	LOCAL	can be “GLOBAL” or “LOCAL”
BACKPHOTO_THICK	24	thickness of the background LOCAL annulus

Table 3: detection set-up for KiDS-ESO-DR3 single-band source lists

The source magnitudes and fluxes in the final source lists are not corrected for Galactic foreground or intergalactic extinction. The result of the S/G classification is available in the source lists via the 2DPHOT flag (SG2DPHOT in the multi-band catalog). Flag values are: 1 (high-confidence star candidates), 2 (objects with FWHM smaller than stars in the stellar locus, e.g., some cosmic-rays and/or other unreliable sources), 4 (stars according to S/G separation), and 0 otherwise (galaxies); flag values are summed, so 2DPHOT = 5 signifies a high-confidence star candidate that is also above the S/G separation line.

#### Multi-band source catalogue

The multi-band source catalogue delivered in this data release is intended as “general purpose” catalogue. The source parameters included in the catalogue are based on double-image mode runs of S-Extractor, where the r-band coadd of each tile is used as detection image and the detection set-up is identical to that used for the single-band source lists (Table 3). Since the r-band image is on average the best quality image for each tile, the S/G separation provided in the catalogue is the same as in the r-band single-band source list. The same masking flags (Table 2) are also included, for each filter. The source magnitudes and fluxes in the catalogue are not corrected for Galactic foreground or intergalactic extinction, but for each source the extinction in each of the 4 filters is provided, interpolated from the extinction maps by Schlegel et al. (1998, ApJ, 500, 525)

To prevent sources in tile overlaps from appearing multiple times in the catalogue, the survey tiles have been cropped to seamlessly connect to each other. Along the edges of survey tiles the data are less deep, but no worse than in the areas located in the gaps between the rows of CCDs in the focal plane, except along the outer edges of the contiguous areas. Since the catalogue is based on detection in the r-band, some sources for which an r-band flux is measured may not have a significant flux in the u, g, or i-band.

## Seeing differences and aperture-matching

Seeing differences between filters are accounted for in two ways:

1. Aperture-corrections; Aperture corrections have been calculated for each filter by comparing the flux in the aperture magnitudes included in the catalogue with the flux in a 6 arcsecond aperture, which is the aperture size used for photometric calibration. The resulting aperture corrections are applied to create the aperture-corrected fluxes included in the catalogue.
2. Gaussian Aperture and Photometry (GAaP) magnitudes; The catalogue includes magnitudes from the PSF homogenization and matched-aperture photometry “GAaP” pipeline. This novel technique is designed to account for PSF differences between different filters, while optimizing signal-to-noise. In short, the PSF within each coadded image is homogenized to a Gaussian shape without significantly degrading the seeing. Aperture photometry is then performed using elliptical Gaussian aperture weight functions, which are analytically corrected for seeing differences. A detailed description of the pipeline can be found in Kuijken et al. (2015, MNRAS, 454, 3500) (K15). It is important to note that these magnitudes are designed for deriving *accurate colours* of galaxies, not for total magnitudes of galaxies. For point sources (stars), GAaP magnitudes approach PSF-fitting photometry.

## Survey photometric homogenization

Zero-point corrections have been calculated for all 440 survey tiles included in the multi-band catalogue to improve the homogeneity of the photometry. These corrections are based on a combination of two methods, namely overlap photometry (OP) and stellar locus regression (SLR). The SLR is used to calibrate the g and i filters to the r-band, and the latter is homogenized over contiguous areas using OP. For u-band the SLR yields poor results and therefore the u-band is homogenized independently using OP.

The majority of stars display a well-defined photometric stellar locus: a tight relation in colour-colour space with a location that varies little across the sky outside the Galactic plane. SLR is the method where the observed stellar locus is matched to the fiducial intrinsic locus, and offers the possibility to achieve colour homogeneity. SLR was applied to the GAaP photometry of unmasked and not flagged, high S/N ( $\text{mag}_{r,\text{GAaP}} < 19$ ) point sources ( $0.4'' < \text{FWHM}_r < 0.8''$ ). Per source the GAaP magnitudes are corrected for Galactic extinction using the E(B-V) colour excess from Schlegel et al. (1998). The stellar locus is parametrized using the “principal colours”  $s$ ,  $x$  and  $w$  as defined by Ivezić et al. (2004, AN, 325, 583). For each of these colours (projections that are linear combinations of the ugri filters), a straight section of the stellar locus lies parallel to one axis (P1) and is centred at 0 on the other axis (P2), see Fig. 5. We add a fourth, redundant colour  $k$  as additional guard for fitting robustness. Per source the P1 and P2 are calculated in each colour and sources on the straight part of the stellar locus are selected using fixed limits in P1. The median P2 values in each tile are converted to zero-point offsets with respect to r ( $d(g-r)$ ,  $d(i-r)$ ). Fig. 5 shows an example of a typical fit.

OP is used to achieve a homogeneous absolute calibration, based on the GAaP photometry of point sources ( $\text{CLASS\_STAR} > 0.8$ ) in the overlaps between adjacent tiles. In the data set used (Fig. 1) 19 contiguous groups are identified, 9 of which are single tiles. A set of criteria, based only on the KiDS data themselves, was derived to identify photometric “anchors” (tiles with accurate photometric calibration). The resulting set of anchors was validated through a comparison with SDSS photometry. According to these criteria 45% of all r-band and 18% of all u-band tiles are consid-

ered anchors to which all other tiles are tied, using a fitting algorithm to minimize the zero-point differences in the overlap regions.

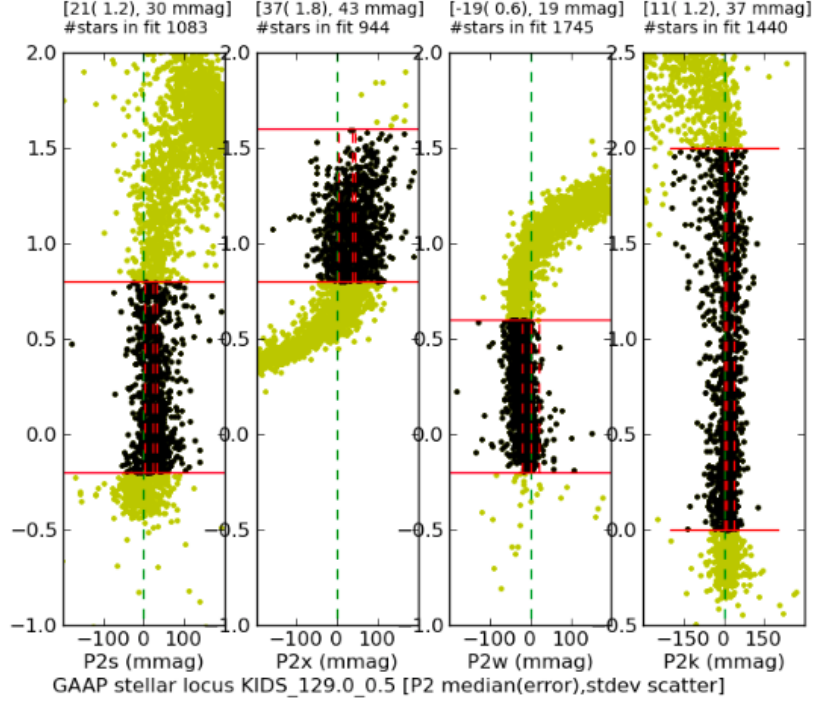


Fig. 5: principal colours  $s, w, x$  and  $k$  for tile  $\text{KiDS}_{129.0\_0.5}$ . The selected stars (yellow) are identical for  $s, w, x$  and  $k$ . From these the stars on the straight section of the locus are selected (black). The inferred median P2 offset, the formal error and standard deviation are shown above each panel.

Combining the results of the SLR and OP yields a zero-point offset / correction per survey tile for each filter. These offsets are included as columns in the multi-band catalogue and can be added to the magnitudes in the catalogue. The offsets are also listed online in the [catalogue table](#).

### colours

Another addition with respect to the catalogue included in the previous data release, is the presence of columns providing source colours. These colours are based on the GAaP magnitudes, which provide the most accurate colours both for galaxies and point sources. Only in these columns the zero-point corrections described above, as well as the Galactic extinction corrections, are already applied.

### Photometric redshifts

Based on the homogenized GAaP photometry, photometric redshifts have been calculated following the methods developed for CFHTLenS and described in K15. This makes use of the Bayesian photometric redshift code BPZ (Benítez, 2000, ApJ, 536, 571) in combination with the re-calibrated templates from Capak (2004, PhD. thesis, Univ. Hawai'i). The best-fit photometric redshift for each source is included in the catalog, while the posterior redshift probability distribution functions (PDFs) are available via the [KiDS-ESO-DR3 website](#). Also included in the catalogue are the ODDS parameter, a measure of the uni-modality of the redshift PDF, and the best-fit template for each source. The values for the latter correspond to the following types, where fractional types can occur because the templates are interpolated: 1=CWW-Ell, 2=CWW-Sbc, 3=CWW-Scd, 4=CWW-Im, 5=KIN-SB3, 6=KIN-SB2.

## Data Quality

An overview of the intrinsic data quality of KiDS-ESO-DR3, in terms of seeing, PSF ellipticity, and limiting magnitudes distributions is presented in Fig. 2. In the following we focus on the quality of the reduced data products.

### Photometric quality

The matter of photometric quality can be split up in two:

1. the uniformity of the photometry within each tile
2. the quality of the absolute photometric calibration per tile/filter

Both the internal photometric homogeneity within a coadd and the quality of the absolute photometric scale can be assessed by comparing the KiDS-ESO-DR3 photometry to SDSS DR8 (Aihara et al., 2011, ApJS, 193, 29). For this, PSF magnitudes were extracted from SDSS DR8 and compared to both the aperture-corrected and GAaP magnitudes in the KiDS-ESO-DR3 multi-band catalogue. Only stars with photometric errors both in KiDS and in SDSS smaller than 0.02 mag in g, r, and i or 0.03 in u were used. This comparison can be done only for all tiles in the KiDS-North field, but since KiDS-South was calibrated in the same way as KiDS-North, we expect the conclusions to hold for all data.

Figure 6 shows the offsets between KiDS aperture-corrected and SDSS DR8 magnitudes for 1 tile (KIDS\_182.0\_-0.5), which is a representative example. Generally, the photometry in a filter is uniform within one tile to within a few percent. In u-band the photometry may be less stable in some cases due to the lack of photometric homogenization within a tile.

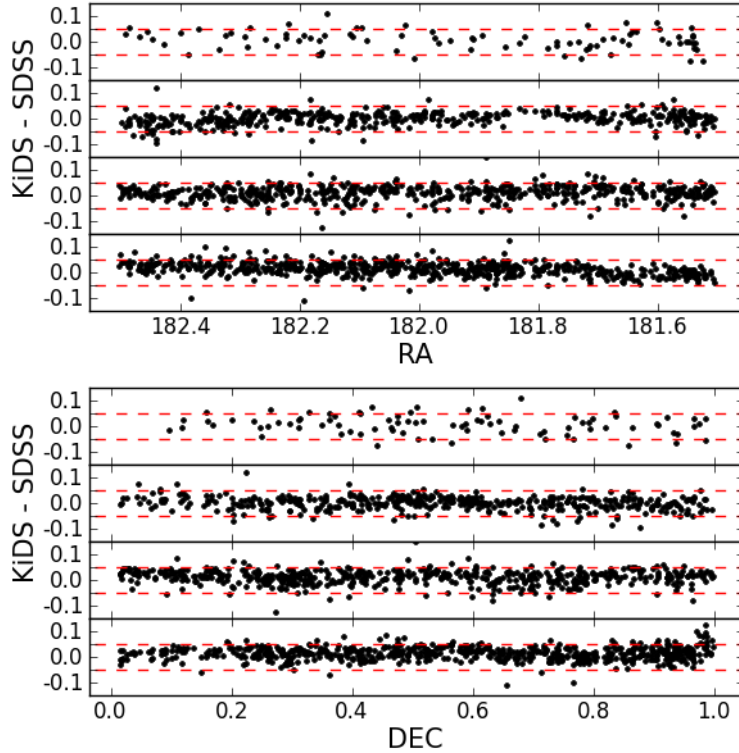


Figure 6: KiDS – SDSS magnitude offsets for (unmasked) stars in tile KiDS 182.0\_-0.5 vs RA (top panel) and DEC (bottom panel), based on aperture-corrected fluxes. From top to bottom the sub-panels correspond to u, g, r, and i, respectively. Each dot corresponds to a star, and the red dashed lines indicate +0.05 and -0.05 magnitudes.

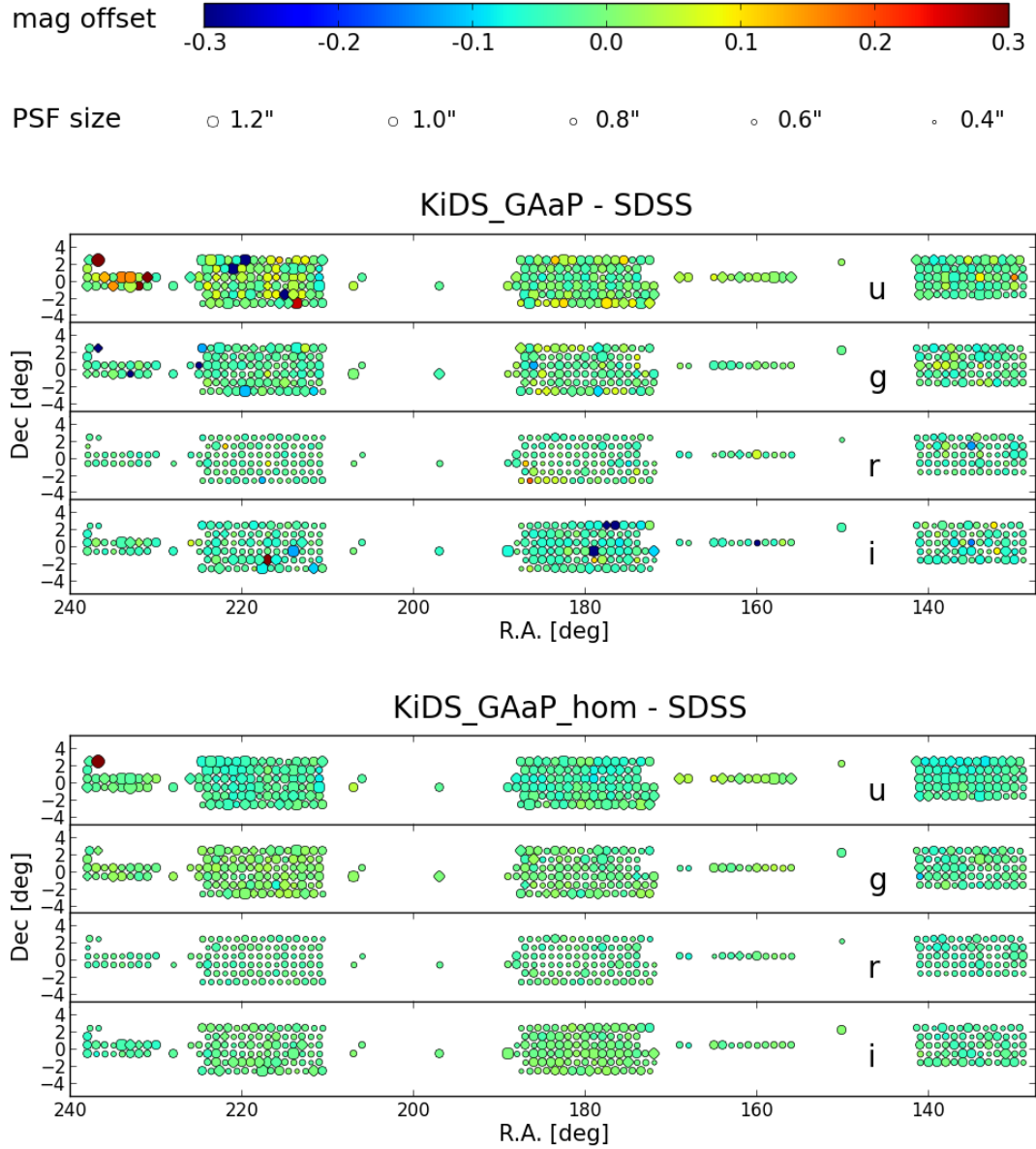


Fig. 7: Photometric calibration and PSF sizes in KiDS-North. Average magnitude offsets for KiDS-ESO-DR3 tiles between KiDS GAaP magnitudes and SDSS DR8 PSF magnitudes of stars are indicated by the colour coding, while the symbol size corresponds to the average PSF size. **Top:** magnitude offsets without photometric homogenization. **Bottom:** magnitude offsets after applying the zero-point corrections from the photometric homogenization.

The quality of the absolute photometric scale is illustrated in Figure 7 and summarized in Table 4. Small systematic offsets of 2 to 3 % are present in all filters. This could be due to the fact that nightly zero-points are determined using a fixed aperture on stars in the SA field without aperture correction. The scatter and occasional outliers in the standard calibration are due to non-photometric conditions (during either KiDS or SA field observations) and, particularly in case of the u-band, use of default zero-points for nights without good SA field observations. Photometric inhomogeneities in SDSS, which is reliable to 1% in gri and 2% in u (Padmanabhan et al. 2008, ApJ, 674, 2) also contribute to the measured scatter.

Filter / colour	Standard calibration				Homogenized calibration			
	Mean offset		Standard deviation		Mean offset		Standard deviation	
	GAaP	Ap.cor	GAaP	Ap.cor	GAaP	Ap.cor	GAaP	Ap.cor
u	0.002	0.051	<b>0.074</b>	<b>0.075</b>	-0.031	0.018	<b>0.033</b>	<b>0.036</b>
g	-0.025	0.017	<b>0.074</b>	<b>0.074</b>	-0.009	0.034	<b>0.024</b>	<b>0.029</b>
r	-0.022	0.016	<b>0.031</b>	<b>0.029</b>	-0.025	0.012	<b>0.015</b>	<b>0.018</b>
i	-0.037	0.015	<b>0.057</b>	<b>0.055</b>	-0.016	0.036	<b>0.018</b>	<b>0.029</b>
s	-0.001	-0.002	<b>0.057</b>	<b>0.057</b>	0.014	0.013	<b>0.017</b>	<b>0.023</b>
w	0.014	0.007	<b>0.041</b>	<b>0.039</b>	-0.002	-0.009	<b>0.004</b>	<b>0.018</b>
x	-0.009	-0.006	<b>0.052</b>	<b>0.051</b>	-0.001	0.002	<b>0.008</b>	<b>0.017</b>

Table 4: Average magnitude offsets and their standard deviation with respect to SDSS DR8 (for u,g,r,i) and expected stellar locus locations (in principal colours s,w,x) for GAaP and aperture-corrected (10'') magnitudes, both before and after photometric homogenization.

The photometric homogenization scheme significantly improves the stability of the calibration and annihilates the outliers completely, with the possible exceptions of isolated tiles or very small contiguous groups without photometric anchors. Derived using GAaP magnitudes, the homogenization clearly works best when applied to the GAaP magnitudes. Given the photometric stability of SDSS quoted by Padmanabhan et al. (2008, ApJ, 674, 2), the standard deviations of the offsets to SDSS (second to last column in Table 4) imply that the stability of the calibration in the u-, g- r- and i-bands is approximately 2%, 2%, 1% and 1%, respectively. Also when applied to the aperture-corrected magnitudes the stability of the calibration is significantly improved and outliers removed. The SLR step in the photometric homogenization procedure ensures that the stellar locus “principal colours” (bottom three rows in Table 4) are close to zero. Overall, the combination of GAaP magnitudes, extinction corrections and photometric homogenization produces the most accurate colours, both for stars and galaxies. Note that the colour columns in the multi-band catalogue already contain all these corrections, while the individual magnitude columns are not corrected for extinction and calibration variations!

#### Photometric redshifts

A quantified measure of the quality of the photometric redshifts in the multi-band source catalogue can be obtained by comparing them to spectroscopic redshifts. Figure 8 shows a direct comparison of best-fit KiDS-ESO-DR3 photometric redshifts ( $z_B$ ) to spectroscopic data from GAMA DR2 (Liske et al. 2015, MNRAS, 452, 2087) and the COSMOS photometric redshift catalogue (Ilbert et al. 2009, ApJ, 690, 1236), where it should be noted that the latter data set overlaps with only one KiDS survey tile (KIDS\_150.1\_2.2). For these comparisons the photometric redshifts of unflagged and unmasked galaxies with  $r < 23$  were characterized by the relative error  $\Delta z = (z_B - z_{\text{spec}}) / (1 + z_{\text{spec}})$ . The comparison with GAMA, mostly restricted to  $z < 0.5$ , yields an outlier rate (here defined as  $|\Delta z| > 0.15$ ) of 1.5%, and after removing these outliers a photo-z bias of 0.02 and scatter of 0.03. Extending to much higher redshifts, the comparison with COSMOS gives an outlier rate of 8.3%, and a photo-z bias and scatter of -0.01 and 0.05, after removal of outliers.

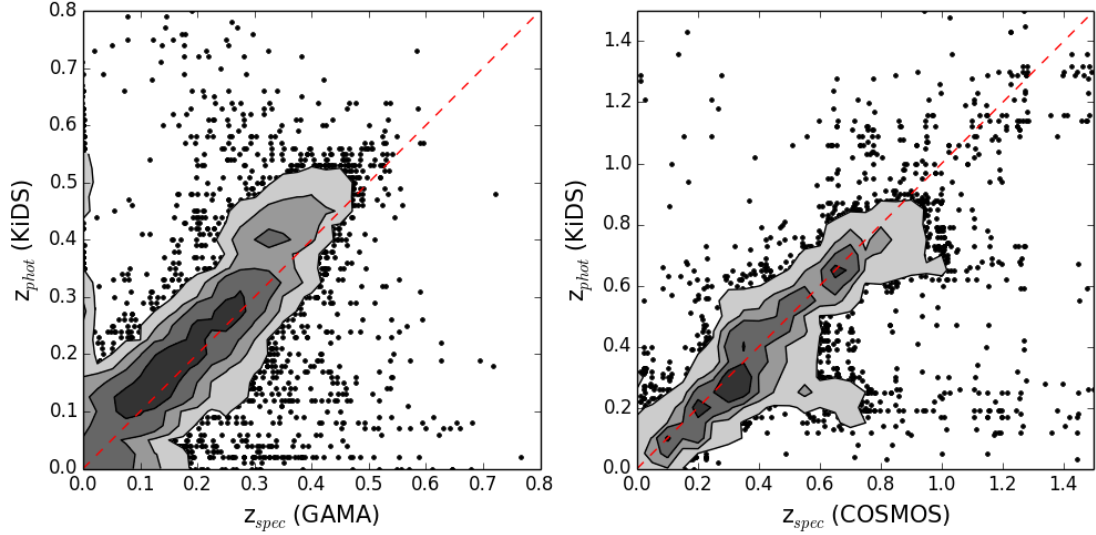


Fig. 8: KiDS photometric redshifts vs. GAMA (left) and COSMOS (right) spectroscopic redshifts. Galaxies are represented by points, which are replaced by contours in the crowded regions of the plots.

#### colour terms

The photometric calibration provided in KiDS-ESO-DR3 is in AB magnitudes in the instrumental system. colour-terms have been calculated with respect to the SDSS photometric system.

Aperture-corrected magnitudes taken from the multi-band catalogue, were matched to SDSS (DR8) PSF magnitudes of point-like sources. For each filter, the median offset to SDSS is first subtracted, rejecting tiles where this offset exceeds 0.1 mag in any of the g, r and i bands. The fit is done on all points from the remaining tiles. The resulting colour terms:

$$\begin{aligned} u_{\text{KiDS}} - u_{\text{SDSS}} &= (-0.050 \pm 0.002) (u_{\text{SDSS}} - g_{\text{SDSS}}), \\ g_{\text{KiDS}} - g_{\text{SDSS}} &= (-0.052 \pm 0.002) (g_{\text{SDSS}} - r_{\text{SDSS}}), \\ r_{\text{KiDS}} - r_{\text{SDSS}} &= (-0.033 \pm 0.002) (g_{\text{SDSS}} - r_{\text{SDSS}}), \\ i_{\text{KiDS}} - i_{\text{SDSS}} &= (+0.012 \pm 0.002) (r_{\text{SDSS}} - i_{\text{SDSS}}). \end{aligned}$$

#### Astrometric quality

The accuracy of the absolute astrometry (“KiDS vs 2MASS”) is uniform over a coadd, with typical 2-dimensional (2-D) RMS of 0.31 arcsec in g, r, and i, and 0.25 arcsec in u. The lower RMS in u-band is most likely due to the fact that in this band on average brighter 2MASS sources are selected as reference sources. The accuracy of the relative astrometry (“KiDS vs KiDS”), measured by the 2-D positional residuals of sources between dithers, is also uniform across a single coadd. In Figure 9 the accuracy of this relative astrometry of all coadds is shown. The typical 2-D RMS is  $\sim 0.03$  arcsec in all filters, but with a larger scatter in u. The larger range in RMS in u-band is due to the smaller number of available reference sources.

#### Completeness and contamination

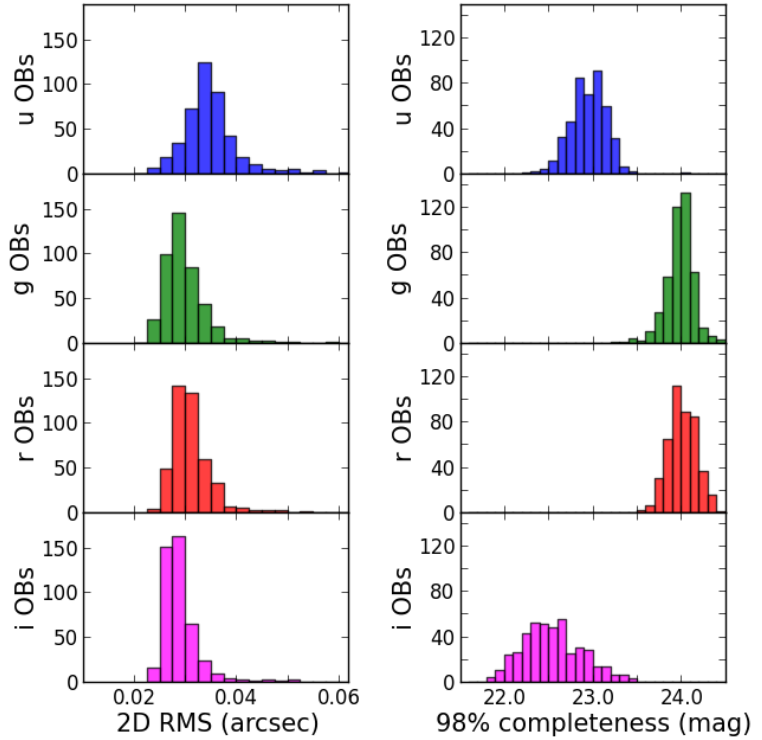
Contamination of the KiDS multi-band catalogue by spurious sources was analysed through a comparison of the overlap between KiDS and the CFHT Legacy Survey (<http://www.cfht.hawaii.edu/Science/CFHLS/>), the main deeper survey overlapping with the current release (CFHTLS-W2, using their final data release T0007). For the analysis it is assumed that all KiDS sources not detected in CFHTLS-W2 are spurious. Since some fraction of real sources might be absent in the CFHTLS catalogues, the spurious fractions derived should be considered upper limits.

Figure 10 shows the spurious fractions derived from this comparison as function of magnitude (r-band  $\text{MAG}_{\text{ISO}}$ ) and signal-to-noise (in a 2" aperture). When all sources in the catalogue are

considered the fraction of spurious sources is estimated to be  $<5\%$  down to a very low SNR of  $\sim 5$  within a  $2''$  aperture. Filtering sources based on masking information reduces this fraction to  $\sim 2\%$ , demonstrating that caution is required when using faint sources in masked regions. When also sources with non-zero SExtractor detection flags are filtered out, the spurious fractions drops even further to  $\sim 1\%$ , yielding a very clean catalogue down to the detection limit.

An internal estimate of the completeness for KiDS-ESO-DR3 is provided per tile, based on the method of Garilli et al. 1999 (A&A, 342, 408). It determines the magnitude at which objects start to be lost in the source list because they are below the brightness threshold in the detection cell. The implementation is similar to La Barbera et al. (2010, MNRAS, 408, 1313). Estimates of the completeness obtained by comparison to deeper CFHTLS-W2 data are consistent with these internally derived values. The distributions of the 98% completeness magnitudes for all tiles are shown in Figure 9. Comparison with Figure 2 shows that the 98% completeness limits are typically  $\sim 1$  magnitude brighter than the limiting magnitude for g, r and i and  $\sim 1.3$  magnitudes brighter in u. For the completeness of the multi-band catalogue the values for the r-band of each tile apply.

Figure 9: Overview of the astrometric quality and completeness of all 440 survey tiles contained in the multi-band catalogue). **Left:** median relative astrometric offsets between the dithers in a coadd. **Right:** 98% completeness magnitude distributions for all tiles. In both columns the panels correspond to u, g, r, and i from top to bottom.



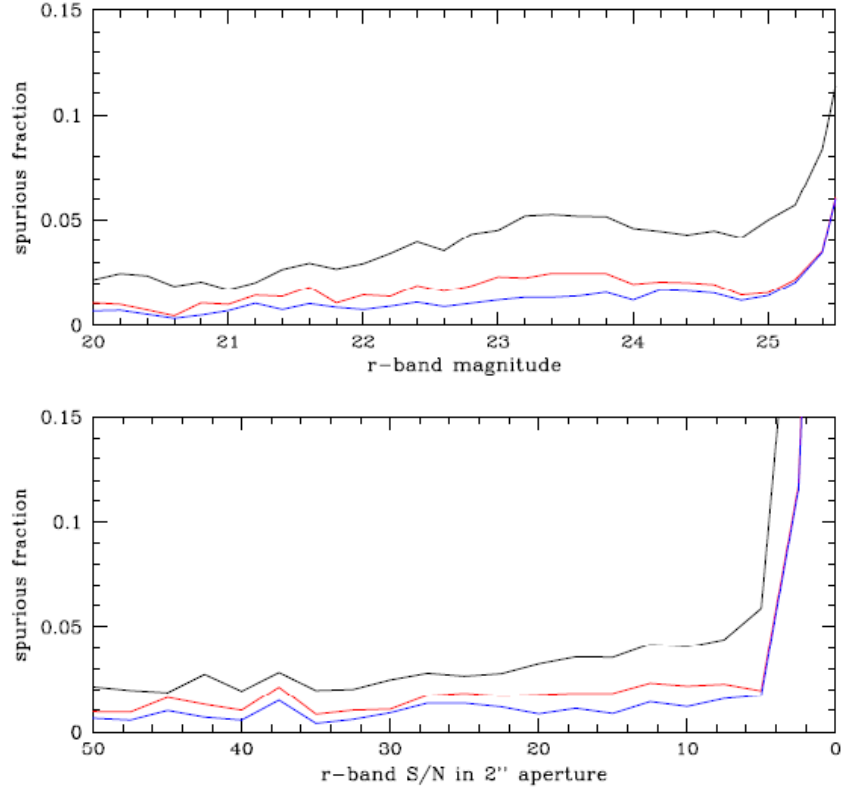


Figure 10: Spurious source contamination in the overlap between KiDS-ESO-DR3 and the CFHTLS-W2 field (this corresponds to the KiDS tiles KiDS\_135.0\_-1.5 and KiDS\_136.0\_-1.5). **Top:** spurious fraction vs. *r*-band magnitude (*MAG\_ISO*). **Bottom:** spurious fraction vs. signal-to-noise in a 2'' aperture. The black line corresponds to all sources, while the red line excludes sources in masked areas, and the blue line excludes sources in masked areas and sources with a non-zero SExtractor flag.

## Known issues

### Image defects

#### Scattered light and reflections

Some of the main issues in the early VST/OmegaCAM data are related to scattered light and reflections. Due to the open structure of the telescope, light from sources outside the field-of-view is often affecting the observations. This expresses itself in a number of ways:

- Reflections: in some cases strong reflected light patterns are seen in the focal plane; these are caused by light from bright point sources outside the field-of-view and can occur in all filters. Some examples are shown in Figure 11a.
- Vignetting by CCD masks: vignetting and scattering by the masks present at the corners of the focal plane array, and at the gaps between the rows of CCDs; this effect is particularly strong in *i*-band due to the bright conditions. The effect near the CCD gaps is largely corrected for, but in many cases the areas in the corners of the CCD array is strongly affected. Examples are shown in Figure 11b.
- Extended background artefacts: related to the reflections mentioned before, this is mostly seen in *i*-band and probably caused by moonlight. An example is shown in Figure 11c.

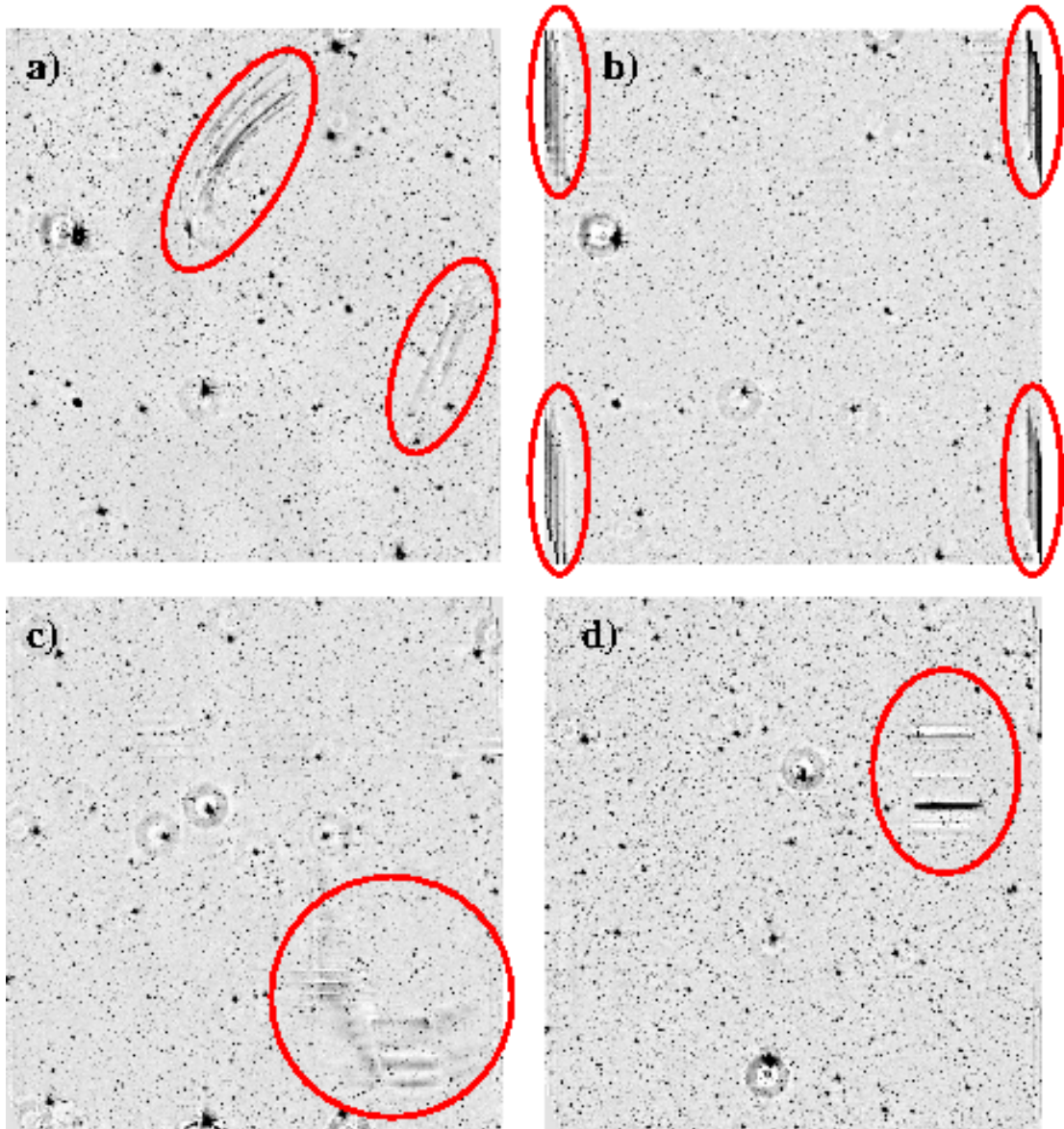


Figure 11: examples known issues in the VST/OmegaCAM data, highlighted by the red ellipses. **a)** light patterns caused by reflections and scattered light of bright sources outside the FOV. **b)** vignetting and scattering by CCD masks at the corners of the CCD array. **c)** extended background structures caused by scattering of moonlight. **d)** patterns caused by defective video board of CCD 82.

Most of these effects are not (yet) corrected for in the current data processing. Automatically generated masks for affected areas are under development and will be provided on the [KiDS-ESO-DR3 website](#) in due course.

Improvements to the telescope baffles that were installed in 2014 and 2015 significantly improve scattered light suppression.

#### Individual CCD issues

There are two issues related to individual CCDs that noticeably affect this data delivery:

- CCD 82: this CCD suffered from random gain jumps and related artefacts until its video board was replaced on June 2 2012. Artefacts as shown in Figure 11d are sometimes visible in the image stacks due to this problem. Photometry in this CCD can be used due to the cross-calibration with neighbouring CCDs in the dithered exposures, but part of the

CCD is lost. These features are included in the image masks and affected sources are flagged.

- CCD 93: during a few nights in September 2011 (Early Science Time) one CCD was effectively dead due to a video cable problem. Table 5 lists the eight observations included in the multi-band catalogue do not include this CCD, affecting seven tiles.

Tile	Affected filter
KIDS_338.8_-32.1	g, i
KIDS_339.8_-33.1	i
KIDS_340.0_-32.1	g
KIDS_340.2_-31.2	g
KIDS_341.2_-32.1	i
KIDS_341.4_-31.2	i
KIDS_342.2_-33.1	i

Table 5: Tiles in which CCD 93 is missing in one or more filters

Images with severe defects are indicated using the “image flag” in the online [data table](#). Also, in the multi-band catalogue sources located in an affected tile are flagged via the TILE\_FLAG column.

#### Star-galaxy separation

In images where the PSF size and shape varies strongly over the field-of-view, the star-galaxy separation provided in the single-band catalogs and the multi-band catalogue can be imperfect. Stars in areas where the PSF is significantly larger than the average for the image can in such cases not be classified correctly.

#### Previous Releases

Preceding the current data release are KiDS data release number 1 (KiDS-ESO-DR1) and number 2 (KiDS-ESO-DR2).

The current release, KiDS public data release number 3 or KiDS-ESO-DR3, contains imaging data and single-band source lists for 292 survey tiles not previously released. Contrary to the previous releases, no manual masking for image defects is included for these tiles.

The multi-band catalog, apart from covering 440 survey tiles compared to 148 in the previous release, contains additional columns, namely:

- Galactic extinction corrections in 4 bands
- matched-aperture “GAaP” magnitudes
- zero-point corrections that homogenize the photometry across tiles
- accurate colours, homogenized and corrected for Galactic extinction
- photometric redshifts

## Data Format

### Files Types

Table 6 lists the types of data products provided in this release, together with descriptions of the file types and naming conventions used.

The naming convention used for all data products is the following:

`KIDS_DR3.0_R.R_D.D_F_TTT.fits`,

where R.R and D.D are the RA and DEC of the tile centre in degrees (J2000.0) with 1 decimal place, F is the filter (u, g, r, or i for single-band data files, ugri for multi-band catalogue files), and TTT is the data product type (see column 4 of Table 6).

For example: the r-band stacked image of the tile “KIDS\_131.0\_-0.5” is called

`KIDS_DR3.0_131.0_-0.5_r_sci.fits`.

Data product	ESO product category name	File type	TTT
Calibrated, stacked images	SCIENCE.IMAGE	FITS image	sci
Weight frames	ANCILLARY.WEIGHTMAP	FITS image	wei
Masks	ANCILLARY.MASK	FITS image	msk
Single-band source lists	SCIENCE.SRCTBL	Binary FITS table	src
Multi-band catalogue data file	SCIENCE.MCATALOG	Binary FITS table	src

Table 6: data products and file types

### Format of coadded images

The final calibrated, coadded images have a uniform pixel scale of 0.2 arcsec. The pixel units are fluxes relative to the flux corresponding to magnitude = 0. This means that the effective zero-point is equal to 0 and the magnitude  $m$  corresponding to a pixel value  $f$  is:

$$m = -2.5 \log_{10} f.$$

### Catalogue Columns

Table 6 lists the columns that are present in the single-band source lists provided in KiDS-ESO-DR3. A large number (27) of aperture fluxes, are provided to suit the needs of different users and allow interpolation to estimate e.g. aperture corrections. Only the columns for the smallest aperture (2 pixels, or 0.4 arcsec diameter) and the largest aperture (200 pixels, or 40 arcsec diameter) are listed in Table 7. Note: the label for the aperture of 28.5 pixels is FLUX\_APER\_28p5.

Table 7 lists the columns that are present in the multi-band source catalogue provided in KiDS-ESO-DR3. Measurements that are provided in each of the four filters are listed only once in the second part of Table 8, where <F> in the label is either 'U', 'G', 'R', or 'I' for the filters u, g, r and i.

Label	Format	Unit	Description
2DPHOT	J		Source classification
X_IMAGE	E	pixel	Object position along x
Y_IMAGE	E	pixel	Object position along y
NUMBER	J		Running object number
CLASS_STAR	E		S-Extractor S/G classifier
FLAGS	J		Extraction flags
IMAFLAGS_ISO	J		FLAG-image flags OR'ed over the iso. profile
NIMAFLAG_ISO	J		Number of flagged pixels entering IMAFLAGS_ISO
FLUX_RADIUS	E	pixel	Fraction-of-light radii
KRON_RADIUS	E	pixel	Kron apertures in units of A or B
FWHM_IMAGE	E	pixel	FWHM assuming a gaussian core
ISOAREA_IMAGE	J	pixel**2	Isophotal area above Analysis threshold
ELLIPTICITY	E		1 - B_IMAGE/A_IMAGE
THETA_IMAGE	E	deg	Position angle (CCW/x)
MAG_AUTO	E	mag	Kron-like elliptical aperture magnitude
MAGERR_AUTO	E	mag	RMS error for AUTO magnitude
ALPHA_J2000	D	deg	Right ascension of barycentre (J2000)
DELTA_J2000	D	deg	Declination of barycentre (J2000)
FLUX_APER_2	E	count	Flux vector within circular aperture of 2 pixels
...	...	...	...
FLUX_APER_200	E	count	Flux vector within circular aperture of 200 pixels
FLUXERR_APER_2	E	count	RMS error vector for flux within aperture of 2 pixels
...	...	...	...
FLUXERR_APER_200	E	count	RMS error vector for flux within aperture of 2 pixels
MAG_ISO	E	mag	Isophotal magnitude
MAGERR_ISO	E	mag	RMS error for isophotal magnitude
MAG_ISOCOR	E	mag	Corrected isophotal magnitude
MAGERR_ISOCOR	E	mag	RMS error for corrected isophotal magnitude
MAG_BEST	E	mag	Best of MAG_AUTO and MAG_ISOCOR
MAGERR_BEST	E	mag	RMS error for MAG_BEST
BACKGROUND	E	count	Background at centroid position
THRESHOLD	E	count	Detection threshold above background
MU_THRESHOLD	E	arcsec**(-2)	Detection threshold above background
FLUX_MAX	E	count	Peak flux above background
MU_MAX	E	arcsec**(-2)	Peak surface brightness above background
ISOAREA_WORLD	E	deg**2	Isophotal area above Analysis threshold
XMIN_IMAGE	J	pixel	Minimum x-coordinate among detected pixels
YMIN_IMAGE	J	pixel	Minimum y-coordinate among detected pixels
XMAX_IMAGE	J	pixel	Maximum x-coordinate among detected pixels
YMAX_IMAGE	J	pixel	Maximum y-coordinate among detected pixels

Label	Format	Unit	Description
X_WORLD	D	deg	Barycentre position along world x axis
Y_WORLD	D	deg	Barycentre position along world y axis
XWIN_IMAGE	E	pixel	Windowed position estimate along x
YWIN_IMAGE	E	pixel	Windowed position estimate along y
X2_IMAGE	D	pixel**2	Variance along x
Y2_IMAGE	D	pixel**2	Variance along y
XY_IMAGE	D	pixel**2	Covariance between x and y
X2_WORLD	E	deg**2	Variance along X-WORLD (alpha)
Y2_WORLD	E	deg**2	Variance along Y-WORLD (delta)
XY_WORLD	E	deg**2	Covariance between X-WORLD and Y-WORLD
CXX_IMAGE	E	pixel**(-2)	Cxx object ellipse parameter
CYY_IMAGE	E	pixel**(-2)	Cyy object ellipse parameter
CXY_IMAGE	E	pixel**(-2)	Cxy object ellipse parameter
CXX_WORLD	E	deg**(-2)	Cxx object ellipse parameter (WORLD units)
CYY_WORLD	E	deg**(-2)	Cyy object ellipse parameter (WORLD units)
CXY_WORLD	E	deg**(-2)	Cxy object ellipse parameter (WORLD units)
A_IMAGE	D	pixel	Profile RMS along major axis
B_IMAGE	D	pixel	Profile RMS along minor axis
A_WORLD	E	deg	Profile RMS along major axis (WORLD units)
B_WORLD	E	deg	Profile RMS along minor axis (WORLD units)
THETA_WORLD	E	deg	Position angle (CCW/world-x)
THETA_J2000	E	deg	Position angle (east of north) (J2000)
ELONGATION	E	deg	A_IMAGE/B_IMAGE
ERRX2_IMAGE	E	pixel**2	Variance of position along x
ERRY2_IMAGE	E	pixel**2	Variance of position along y
ERRXY_IMAGE	E	pixel**2	Covariance of position between x and y
ERRX2_WORLD	E	deg**2	Variance of position along X-WORLD (alpha)
ERRY2_WORLD	E	deg**2	Variance of position along Y-WORLD (delta)
ERRXY_WORLD	E	deg**2	Covariance of position X-WORLD/Y-WORLD
ERRCXX_IMAGE	E	pixel**(-2)	Cxx error ellipse parameter
ERRCYY_IMAGE	E	pixel**(-2)	Cyy error ellipse parameter
ERRCXY_IMAGE	E	pixel**(-2)	Cxy error ellipse parameter
ERRCXX_WORLD	E	deg**(-2)	Cxx error ellipse parameter (WORLD units)
ERRCYY_WORLD	E	deg**(-2)	Cyy error ellipse parameter (WORLD units)
ERRCXY_WORLD	E	deg**(-2)	Cxy error ellipse parameter (WORLD units)
ERRA_IMAGE	E	pixel	RMS position error along major axis
ERRB_IMAGE	E	pixel	RMS position error along minor axis
ERRA_WORLD	E	deg	World RMS position error along major axis
ERRB_WORLD	E	deg	World RMS position error along minor axis
ERRTHETA_IMAGE	E	deg	Error ellipse pos. angle (CCW/x)
ERRTHETA_WORLD	E	deg	Error ellipse pos. angle (CCW/world-x)
ERRTHETA_J2000	E	deg	J2000 error ellipse pos. angle (east of north)
FWHM_WORLD	E	deg	FWHM assuming a gaussian core
ISO0	J	pixel**2	Isophotal area at level 0

Label	Format	Unit	Description
ISO1	J	pixel**2	Isophotal area at level 1
ISO2	J	pixel**2	Isophotal area at level 2
ISO3	J	pixel**2	Isophotal area at level 3
ISO4	J	pixel**2	Isophotal area at level 4
ISO5	J	pixel**2	Isophotal area at level 5
ISO6	J	pixel**2	Isophotal area at level 6
ISO7	J	pixel**2	Isophotal area at level 7
SLID	K		Source list ID
SID	K		Source ID within the source list
HTM	K		Hierarchical Triangular Mesh (level 25)
FLAG	K		Not used

Table 7: columns provided in the KiDS-ESO-DR3 single-band source lists

Label	Format	Unit	Description
<b>Measurements based on r-band detection image</b>			
ID	25A		Source identifier
RAJ2000	D	deg	Right ascension
DECJ2000	D	deg	Declination
SG2DPHOT	K		Star/galaxy separation
A	D	pixel	Linear semi major axis
B	D	pixel	Linear semi minor axis
CLASS_STAR	E		SExtractor star/galaxy classifier
ELLIPTICITY	E		Ellipticity
KRON_RADIUS	E	pixel	Kron-radius used for MAG_AUTO
POSANG	E	deg	Position angle
A_GAAP	D	arcsec	Linear semi major axis of GAaP aperture
B_GAAP	D	arcsec	Linear semi minor axis of GAaP aperture
POSANG_GAAP	E	deg	Position angle of GAaP aperture
<b>Measurements provided for each filter</b>			
FLUX_APER_4_<F>	E	count	flux in 4 pixel aperture
FLUX_APER_6_<F>	E	count	flux in 6 pixel aperture
FLUX_APER_10_<F>	E	count	flux in 10 pixel aperture
FLUX_APER_14_<F>	E	count	flux in 14 pixel aperture
FLUX_APER_25_<F>	E	count	flux in 25 pixel aperture
FLUX_APER_40_<F>	E	count	flux in 40 pixel aperture
FLUX_APER_100_<F>	E	count	flux in 100 pixel aperture
FLUXERR_APER_4_<F>	E	count	flux error in 4 pixel aperture
FLUXERR_APER_6_<F>	E	count	flux error in 6 pixel aperture
FLUXERR_APER_10_<F>	E	count	flux error in 10 pixel aperture
FLUXERR_APER_14_<F>	E	count	flux error in 14 pixel aperture
FLUXERR_APER_25_<F>	E	count	flux error in 25 pixel aperture
FLUXERR_APER_40_<F>	E	count	flux error in 40 pixel aperture
FLUXERR_APER_100_<F>	E	count	flux error in 100 pixel aperture
FLUX_APERCOR_4_<F>	E	count	corrected flux from 4 pixel aperture

Label	Format	Unit	Description
FLUX_APERCOR_6_<F>	E	count	corrected flux from 6 pixel aperture
FLUX_APERCOR_10_<F>	E	count	corrected flux from 10 pixel aperture
FLUX_APERCOR_14_<F>	E	count	corrected flux from 14 pixel aperture
FLUX_APERCOR_25_<F>	E	count	corrected flux from 25 pixel aperture
FLUXERR_APERCOR_4_<F>	E	count	corrected flux error from 4 pixel aperture
FLUXERR_APERCOR_6_<F>	E	count	corrected flux error from 6 pixel aperture
FLUXERR_APERCOR_10_<F>	E	count	corrected flux error from 10 pixel aperture
FLUXERR_APERCOR_14_<F>	E	count	corrected flux error from 14 pixel aperture
FLUXERR_APERCOR_25_<F>	E	count	corrected flux error from 25 pixel aperture
FLUX_RADIUS_<F>	E	pixel	SExtractor FLUX_RADIUS
FWHM_IMAGE_<F>	E	pixel	SExtractor FWHM_IMAGE
FLAG_<F>	J		SExtractor extraction flag
IMAFLAGS_ISO_<F>	J		mask flag
MAGERR_AUTO_<F>	E	mag	error in MAG_AUTO
MAGERR_ISO_<F>	E	mag	error in MAG_ISO
MAG_AUTO_<F>	E	mag	MAG_AUTO
MAG_ISO_<F>	E	mag	MAG_ISO
NIMAFLAGS_ISO_<F>	J		number of masked pixels
ISOAREA_IMAGE_<F>	J	pixel**2	isophotal aperture
XPOS_<F>	E	pixel	X pixel position in image
YPOS_<F>	E	pixel	Y pixel position in image
MAG_GAAP_<F>	E	mag	GAaP magnitude
MAGERR_GAAP_<F>	E	mag	error in GAaP magnitude
ZPT_OFFSET_<F>	E	mag	glob.phot. ZPT offset
EXT_SFD_<F>	E	mag	Galactic foreground extinction following Schlegel et al. maps
<b>Other columns</b>			
SCID	K		Astro-WISE SourceCollection identifier
SLID	K		Astro-WISE SourceList identifier
SID	K		Astro-WISE Source identifier
Z_B_BPZ	E		Best-fitting BPZ photometric redshift
ODDS_BPZ	E		Empirical ODDS of Z_B_BPZ
T_B_BPZ	E		Best-fitting BPZ spectral type
TILE_FLAG	J		Tile quality warning flag
colour_GAAPHOM_U_G	E	mag	Homogenized and Extinction corrected GAaP u-g band colour
colour_GAAPHOM_U_R	E	mag	Homogenized and Extinction corrected GAaP u-r band colour
colour_GAAPHOM_U_I	E	mag	Homogenized and Extinction corrected GAaP u-i band colour
colour_GAAPHOM_G_R	E	mag	Homogenized and Extinction corrected GAaP g-r band colour
colour_GAAPHOM_G_I	E	mag	Homogenized and Extinction corrected GAaP g-i band colour
colour_GAAPHOM_R_I	E	mag	Homogenized and Extinction corrected GAaP r-i band colour

Table 8: columns provided in the KiDS-ESO-DR3 multi-band catalogue.

## Acknowledgements

The following acknowledgment is valid at the moment of writing this document. For an up-to-date version, please visit the following webpage: <http://kids.strw.leidenuniv.nl/DR3/acknowledgements.php>

Users of data from this release should cite “de Jong et al. (2013, ExA 35, 25)”.

Please use the following statement in your articles when using these data:

*Based on data products from observations made with ESO Telescopes at the La Silla Paranal Observatory under programme IDs 177.A-3016, 177.A-3017 and 177.A-3018, and on data products produced by Target/OmegaCEN, INAF-OACN, INAF-OAPD and the KiDS production team, on behalf of the KiDS consortium. OmegaCEN and the KiDS production team acknowledge support by NOVA and NWO-M grants. Members of INAF-OAPD and INAF-OACN also acknowledge the support from the Department of Physics & Astronomy of the University of Padova, and of the Department of Physics of Univ. Federico II (Naples).*